

Modeling and Monitoring of a Distillation Column

Samia Latreche*, Mohammed Mostefai, Abd Essalam Badoud, Mabrouk Khemliche
Automatic Laboratory – LAS, Electrical Engineering Department
Faculty of Technology, University of Setif 1
Setif, Algeria

*Email: ksamia2002 {at} 47yahoo.fr

Abstract—This paper presents the development of a real-time monitoring solution for a complex distillation column UOP3BM Armfield. A predictive controller was created and associated with a bond graph model. The developed solution was designed to track the time-varying and the non-stationary dynamics of the process. Furthermore, to improve the isolation capabilities, a bond graph approach was applied. Experimental results are given to support the theoretical development.

Keywords-modeling; monitoring; distillation column; sensors placement.

I. INTRODUCTION

Distillation columns are widely used in chemical processes and exhibit a nonlinear dynamic behavior, making its optimal performance dependent on an effective control strategy [1]. In recent years, model-based control strategies such as an internal model control (IMC) and model predictive control (MPC) have been shown to have very promising results in comparison with conventional methods [2]. However, their major challenge lies in building a model capable of describing the process under consideration [3]. An example of a recent modeling technique capable of taking into account the physical coupling of the column is the use of artificial neural networks [4]. The drawback of this technique is that the neural networks are approximate models. For a practical usage, another technique called “Wiener model” has been used in order to solve the nonlinearities in the distillation processes [5]

The complex and non-linear nature of several issues of Chemical Engineering is frequently described by phenomenological or empirical models represented by the non-linear algebraic equations [6]. Bond graph models of steady-state reactive distillation involve the solution of a system of the nonlinear equations. The equation’s non-linearity is mainly produced from equations used in the modeling of phase equilibrium and from those used for the calculation of the reaction.

Another issue related to model-based control strategy is monitoring. To limit the use of sensors, soft sensors established themselves as a valuable alternative to the traditional means for acquiring critical process data, to process monitoring and to other tasks which are related to process control [7]. A soft sensor is a model which is used to estimate the non-measurable output of an industrial process, it is very useful in

process control because it can be used to control and monitor many industrial processes [8]. However, the design of the soft sensor is difficult due to the modeling is often based on case data. These data have the features of discreteness, nonlinearity, contradiction, and complexity [9], [10].

In this work, both bond graph modeling and soft sensor use are proposed for distillation columns. Thus, section 2 will describe the model of the distillation column, section 3 will present its experimental equivalent and section 4 will cross-compare simulation results with measurements. Based on this model, the problem of optimal placement of sensors will be treated in section 5 and simulated in section 6. Finally, section 7 will present the conclusions of the work.

II. USING BOND GRAPHS TO MODEL A DISTILLATION COLUMN

The bond graph methodology as a multi-disciplinary, graphical and unified modeling language well suited for problems such as the distillation column [8], [9]. It attempts to model a system using power flows under the assumption that there exists fundamentally a similar relationship between power conjugates.

Bond graph models are ideally suited for modeling a nonlinear system. A bond graph model does not assume any linearity constraints. The model hides the complexity of nonlinearity from the user of the model. Once the modeler defines the nonlinear relationship in the model, it is the job of the underlying bond graph software to solve the model. The whole process is transparent to the user of the model.

1-port element is the most basic of the bond graph elements. This element has a single port for energy exchange with its environment. There will be a constitutive equation depicting the relationship between the co-variables of the element bond.

The only constraint on the constitutive equation is that the energy should be conserved as per the underlying physical law of bond graph modeling. Two different relationships between the co-variables (effort and flow) are depicted graphically in Figure (1-a) and (1-b). The bond graph model for this relationship is depicted by 1-port elements in Figure (1-c).

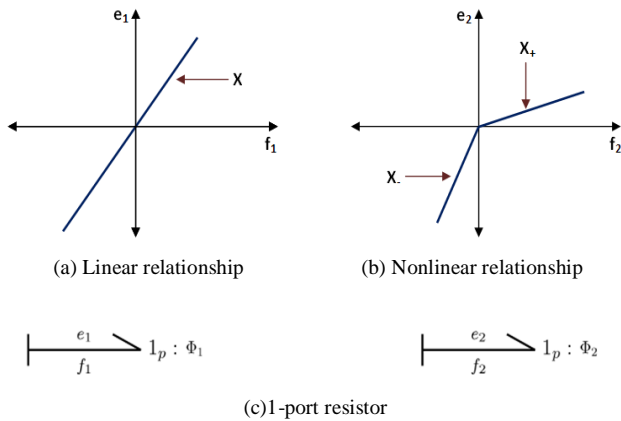


Figure 1. Relationship between flow and effort for 1-port resistor elements

The constitutive relationship for the 1-port resistor elements are given in equations (1) and (2). It can be seen that the model for both linear and nonlinear behavior look-alike, with the constitutive relationship hiding the difference. It is the job of the solver software to simulate the model differently.

$$e_1 = \phi_1 f_1 \quad (1)$$

$$e_2 = \phi_2(f_2) \quad (2)$$

$$\text{where, } \begin{cases} \phi_1 = X & \text{always} \\ \phi_2 = X_- & \text{if } f_2 < 0 \\ \phi_2 = X_+ & \text{if } f_2 > 0 \end{cases} \quad (3)$$

Bond graph provides a simple approach for modeling complex systems, which allows both a structural and a behavioral system analysis.

The advantages of applying bond graph models to distillation columns are the ability to build a graphic for the entire system, the use of detailed equations, the encapsulation of pieces of the model into sub-models and the representation of the system power flows in detail. The main drawback of using bond graphs is that they cannot describe distillation equations. Their convection bonds must be modified causing the model be less precise and slower to converge [11].

A. Assumptions

The following assumptions are made in the bond graph model proposed in this work:

- The process has reached steady state.
- The liquid composition at each stage is homogeneous and equal to the composition of the liquid leaving the stage.
- The vapor and liquid leaving at any stage are in physical equilibrium.
- The vapor molar holdup and vapor-phase chemical reactions were neglected.

The distillation column is composed by condenser, reboiler and plates. For the elaboration of the global bond graph model of distillation column we proceed as follows:

- We devise the global system on subsystem
- We elaborate the bond graph model for each subsystem
- We associate these subsystem models in global model
- We simplify the global model.

B. Bond graph Model of the Distillation Column

Steam condensation involves both convection and conduction. In process engineering systems, it is simpler to use enthalpy flow instead of entropy flow to model heat convection using pseudo-bond graph representation. In this paper, pressure and temperature are considered as the generalized effort variables, and mass flow rate and enthalpy flow rate are taken as the generalized flow variables. The convection heat transfer due to mass flow is represented using inter-domain couplings.

The column is composed by the reboiler, the plates and the condenser. The bond graph of each component is as follows:

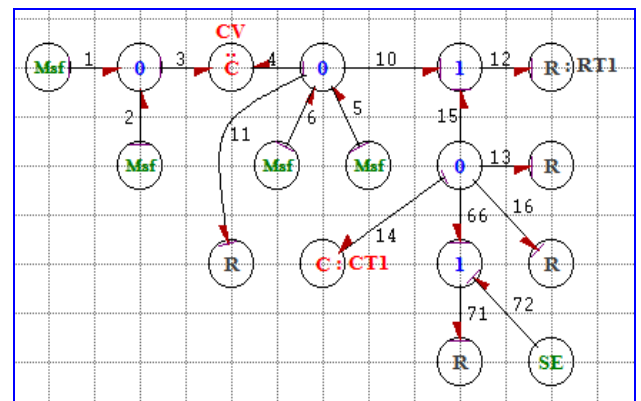


Figure 2. Bond graph model of the reboiler

The reboiler and part of the base are shown in the bond graph of figure (1). The entropy flows from the steam header into the steam chamber to the metal of the tubes and into the reboiler chamber. The reboiler chamber is considered to affect the entire base, and so the rightmost 0-nodes of figure (2) show only some of the required bonds. Not shown are the effects of the liquid and the vapor leaving or coming into the base. Unlike the other valves in the system, the steam valve is modeled as an R element. All valves could be modeled as R elements, but the hydraulic power flow into thermal power is usually considered negligible. The C:CV element assumes that the pressure is high enough (as would be typical in a steam header) that the density of the steam is not dependent on pressure, but on temperature alone. If the steam were not considered incompressible, the C:CV element would be replaced by a C element

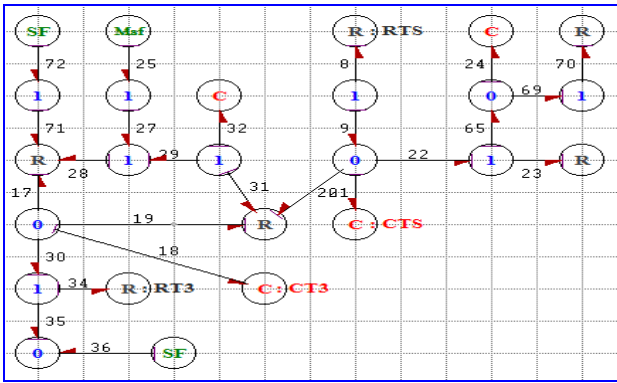


Figure 3. Bond graph model of the plates

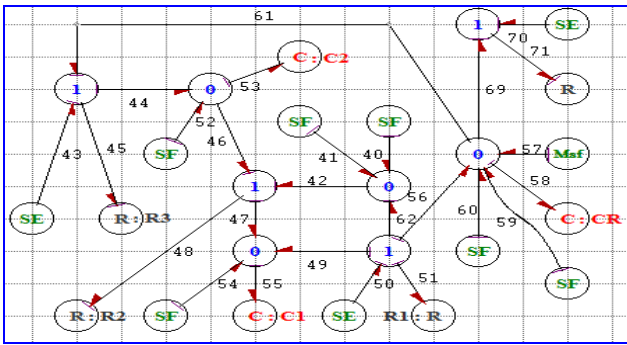


Figure 4. Bond graph model of the condenser

The proposed model is shown in Fig. 5. Its components are listed in Table I.

TABLE I. MODEL COMPONENTS

Component name	Component symbol
CT _i	Ith Tank capacitor
CI	Liquid capacitor
CV	Vapor capacitor
CTS	Output tank capacitor
C _i	Ith Pipe
CR	Restriction capacitor
RT _i	ith Tank resistor
RTS	Separation resistor
R _i	Ith Valve
E	Effort
F	Flow
SE	Effort source
SF	Flow source
MSf	Modulated flow source
0	Junction of common effort
1	Junction of common flow

The bond graph model of the distillation column is given by Fig. 5.

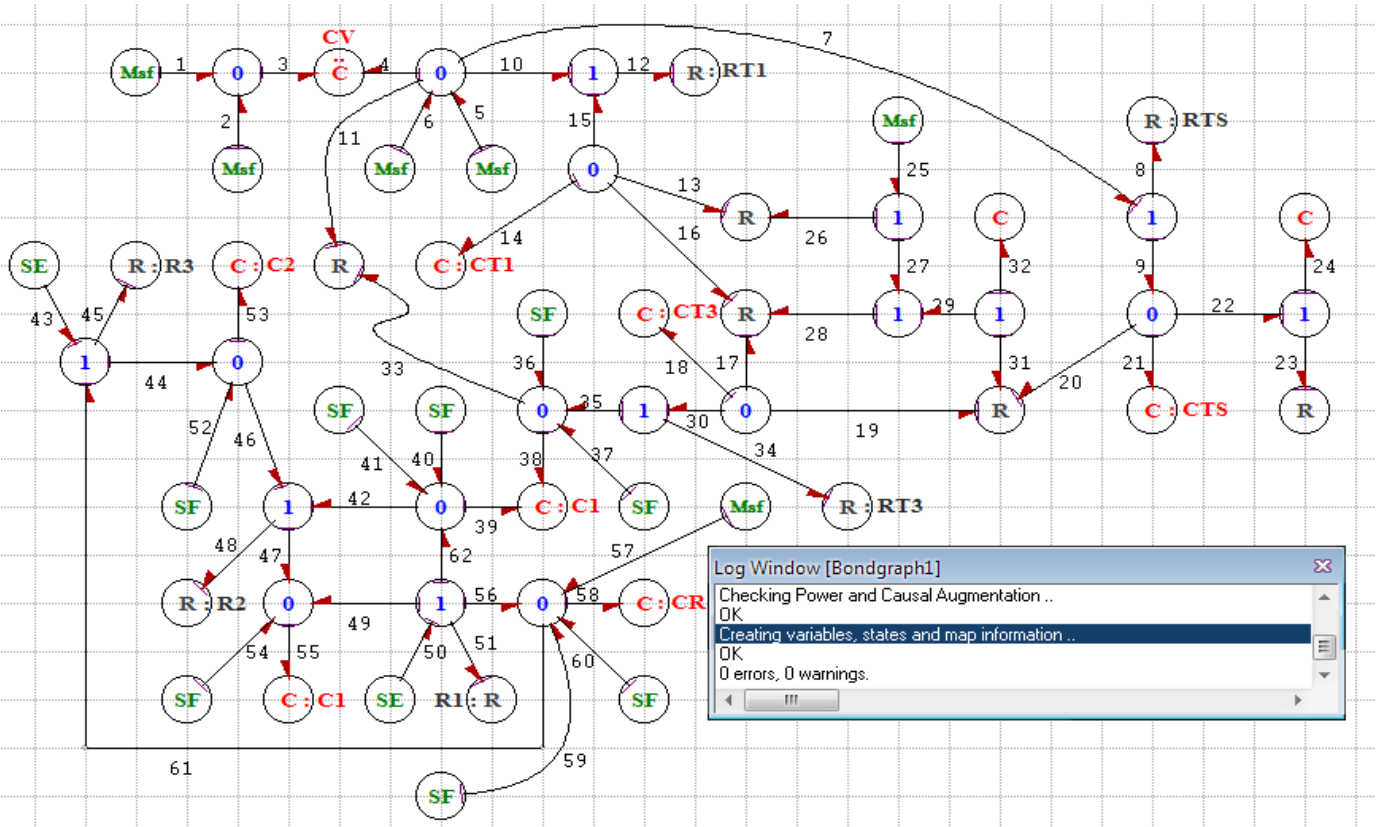


Figure 5. Bond graph model of distillation column

The modeling objective is an accurate prediction of overhead and bottoms product composition for changes in the reboiler steam rate and reflux rate.

III. EXPERIMENTAL TEST

The experimental bench used in this work is a distillation column built in a pilot-scale. The purpose of the experiments is to determine the operating conditions of a five-plate distillation column used to separate a liquid binary mixture of water and ethanol (10-20%) into a distillate product with ethanol (75-88%) and bottom product with (92 - 98%) water (mole fractions).

The column is composed by several glass sections supported by an external steel framework. In order to guarantee minimal heat loss to the surroundings the glass sections are enfolded with proper isolation material.

This distillation column takes a considerable amount of time to reach steady-state which extends the experiment time to around 3 hours.

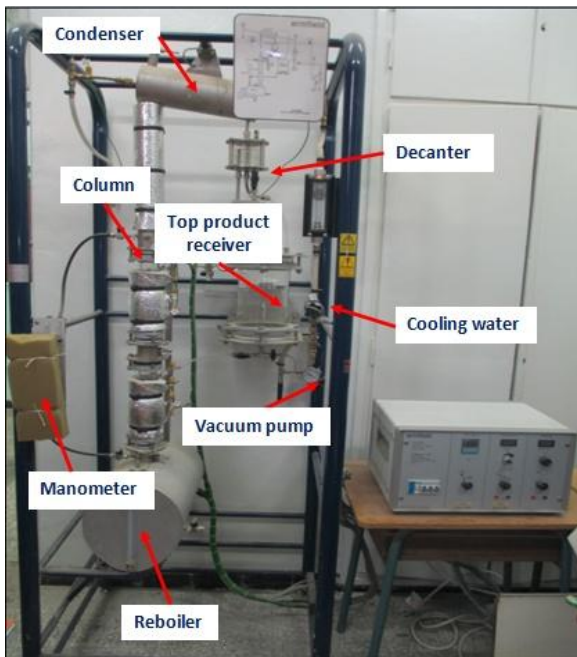


Figure 6. Pilot scale distillation column

The column measurement instrumentation consists of two types of sensors: temperature thermocouple type T, and pressure sensors type P. These sensors gather real-time information about temperature and pressures at different points in the column. Its actuators consist of: heater elements, valves and peristaltic pumps.

The digital controller operates the measurement, actuator and network communication systems through the Field Point I/O bus. The control systems was designed and run using a LabView interface. The composition of both the distillate and the bottom product are inferred through the density of feed, distillate and residue samples collected offline.

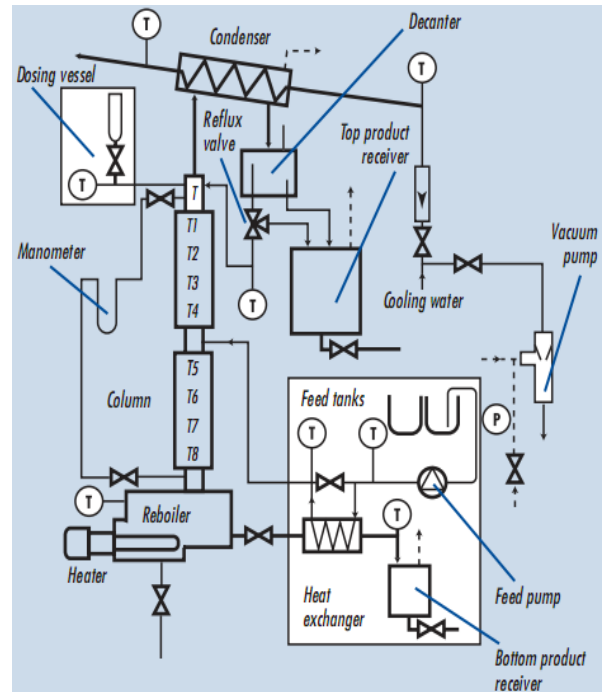


Figure 7. Column measurement instrumentation

The distillation process starts with the liquid feed mixture being pre-heated using an automatic controller 1200W electrical heater. A fraction of the condensed distillate ethanol, leaving the top section, is feed backed into the column at a rate determined by the actuation of a solenoid reflux valve. The liquid mixture travels downwards through the section below the feeder and into the reboiler. Here, part of the mixture changes phase from liquid to vapor under the heat of two automatically controlled 2000W electrical ON/OFF heater elements. This water-rich mixture leaves the bottom section of the column through a condenser before being stored in the product tank.

The distillation operation is repeated for three different rates of reflux (1, 2 and 4). The refractive index of the distillate and residue is measured to determine the effect of the reflux ratio on the quality of each distillation. The results obtained are presented in the Table II.

TABLE II. THE REFRACTIVE INDEX OF COLUMN DISTILLATE FOR EACH TEST

TEST	REFLUX RATIO	IR _R	x _R	IR _D	x _D
1	1	1.336225	10.02	1.329	100
2	2	1.336225	10.02	1.329	100
3	4	1.336225	10.02	1.329	100

Where x_D is the mole fraction of the distillate and x_R is the mole fraction of the residue. The efficiency of the column can be calculated from (4).

$$\eta = \frac{\text{Number of theoretical plates}}{\text{Number of practical plates}} = \frac{N}{N_R} \quad (4)$$

The number of theoretical plates can be calculated from (5)

$$N = \frac{\ln\left(\frac{x_d}{1-x_d}\right)\left(\frac{1-x_r}{x_r}\right)}{\ln(\alpha_{avg})} - 1 \quad (5)$$

The α_{avg} is the average relative volatility of the more volatile component to the less volatile one. For ease of expression, the more volatile component is referred to as light key (LK) while the less volatile one is referred to as heavy key (HK). Using this terminology, the above equation may be expressed as (6):

$$N = \frac{\ln\left(\frac{LK_d}{1-LK_d}\right)\left(\frac{1-LK_b}{LK_b}\right)}{\ln(\alpha_{avg})} - 1 \quad \text{or} \quad N = \frac{\ln\left(\frac{LK_d}{HK_d}\right)\left(\frac{HK_b}{LK_b}\right)}{\ln(\alpha_{avg})} - 1 \quad (6)$$

If the relative volatility of the LK to the HK is constant from the column top to the column bottom, then α_{avg} is simply α . If this is not the case, the approximation in (7) may be used.

$$\alpha_{avg} = \sqrt{(\alpha_t)(\alpha_b)} \quad (7)$$

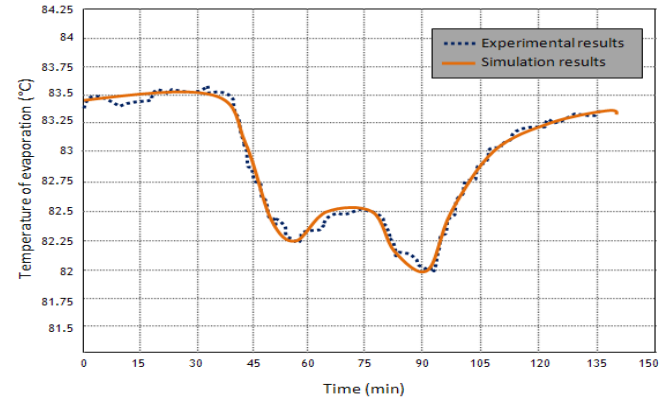
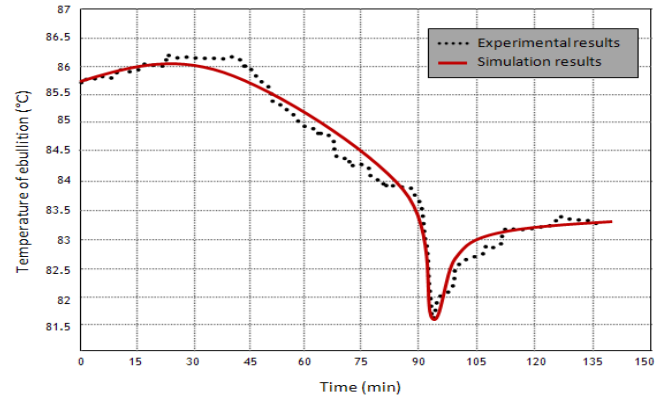
Where α_t is the relative volatility at top of column; α_b is the relative volatility at bottom of column.

IV. SIMULATION AND EXPERIMENTAL RESULTS

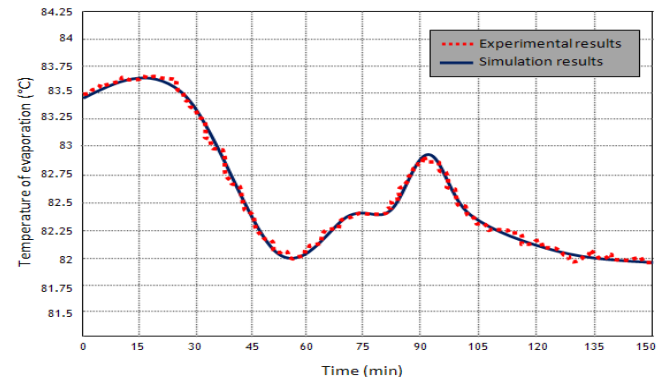
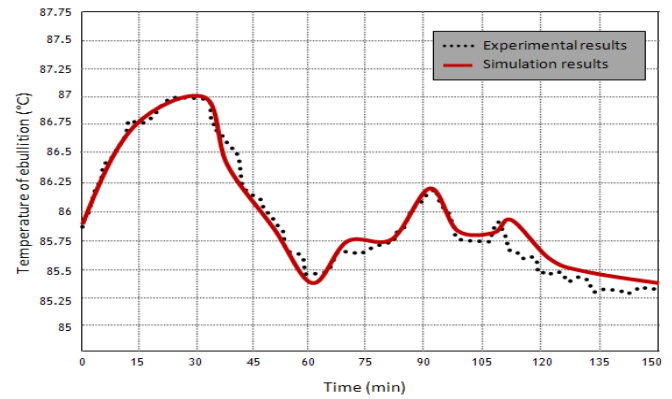
The data obtained from the simulations and the experiments will be compared in order to validate the consistency of the proposed model which is represented by Table III.

TABLE III. VARIANCE ACCOUNTED FOR VALUES FOR THE BOND GRAPH MODEL BASED ON EXPERIMENTAL AND SIMULATED DATA

	T_{ebul}		T_{vap}	
	Simulated	Measured	Simulated	Measured
June 1 st	99.35	98.46	48.73	44.03
June 2 nd	96.43	99.86	77.97	89.69
June 3 rd	97.03	99.32	56.22	58.77
June 4 th	97.85	99.73	44.86	66.72
June 5 th	97.28	99.94	51.41	70.11
June 8 th	96.44	99.77	75.79	88.07
June 11 th	98.62	98.67	59.84	48.20
June 15 th	98.11	98.73	41.07	50.65



(a) June 2nd, 2014



(b) June 8th, 2014

Figure 8. Overlaid estimated outputs from the simulation based models to the real experiments

recently [11]. In this work, the method for optimizing sensor placement will be based on the bond graph model. Its objective is to minimize the number of sensors but monitor all the components.

Consider a given bond graph model obtained from a physical process without sensors. Let x_i and y_j be the binary variables to express the potential sensor placement on the junction nodes such as:

$$x_i = \begin{cases} 1 & \text{if the } i^{\text{th}} \text{ sensor is placed on the } i^{\text{th}} \text{ "0"} \\ 0 & \text{otherwise} \end{cases} \quad (8)$$

$$\begin{cases} \sum_{k=1}^{n_i} a_k f_k = 0 \\ e_k = e_{C_i} \end{cases} \quad \text{where } k = 1, n_i - 1 \quad a_i = \begin{cases} 1 & \text{if the half-arrow is toward junction} \\ 0 & \text{otherwise} \end{cases} \quad (10)$$

Similarly, equations of the j^{th} "1" junction are shown in (11):

$$\begin{cases} \sum_{l=1}^{m_j} a_l f_l = 0 \\ f_l = f_{R_j} \end{cases} \quad \text{where } k = 1, m_j - 1 \quad a_l = \begin{cases} 1 & \text{if the half-arrow is toward junction} \\ 0 & \text{otherwise} \end{cases} \quad (11)$$

Two sets of variables can be defined by equations (12) and (13).

$$K = MSe \cup MSf \cup De \cup Df \cup u \quad (12)$$

The set K relates to the known variables and contains the control variables u , the variables whose value are measured by sensors, the controlled (MSe , MSf) and perturbation (Se , Sf) sources.

$$X(t) = \{e_1(t), f_1(t)\} \cup \{e_2(t), f_2(t)\} \dots \{e_n(t), f_n(t)\} \quad (13)$$

Where n is the number of bond graph R , C and I elements.

Based on the causal properties of the bond graph modeling, the unknown variables can be calculated using covering causal paths. For the "0" and the "1" junction, the unknown variable (based on fixed causality) is calculated by equations (14) to (16).

$$\begin{cases} f_{C_i} = \phi_{C_i} [s \{ (1-x_i)(e_{C_i}) + x_i De_i \}] \\ e_{C_i} = \frac{1}{s} (1-x_i) \phi_{C_i}^{-1} (f_{C_i}) + x_i De_i \end{cases} \quad \text{where } i = 1..N \quad (14)$$

$$\begin{cases} e_{R_j} = \phi_{R_j} [(1-y_j)(f_{R_j}) + y_j Df_j] \\ f_{R_j} = (1-y_j) \phi_{R_j} (e_{R_j}) + y_j Df_j \end{cases} \quad \text{where } j = 1..N_1 \quad (15)$$

$$\begin{cases} e_{L_k} = \phi_{L_k} [s(1-z_k)(f_{L_k}) + z_k Df_k] \\ f_{L_k} = \frac{1}{s} (1-z_k) \phi_{L_k} (e_{L_k}) + z_k Df_k \end{cases} \quad \text{where } k = 1..N_1 \quad (16)$$

$$y_j = \begin{cases} 1 & \text{if the } j^{\text{th}} \text{ sensor is placed on the } j^{\text{th}} \text{ "1"} \\ 0 & \text{otherwise} \end{cases} \quad (9)$$

Where N_0 is the number of "0" junctions, N_1 is the number of "1" junctions, n_i is the number of bonds around the i^{th} "0" junction ($i = 1, N_0$), n_j is the number of bonds around the j^{th} "1" junction ($j = 1, N_1$).

Equations of the i^{th} "0" junction are described by (10), where "f" is the flow vector and "e" is the effort vector.

The equations at the junctions "0" and "1" are denoted by (17) and (18).

$$\begin{cases} e_3 = e_2 = e_1 \\ f_1 + f_2 - f_3 = 0 \\ f_{CV} = f_3 = \phi_{CV} [s \{ (1-x_1)e_3 + x_1 De_1 \}] \\ e_{CV} = e_3 = \frac{1}{s} (1-x_1) \phi_{CV}^{-1} (f_3) + x_1 De_1 \end{cases} \quad (17)$$

$$\begin{cases} f_{10} = f_{12} = f_{15} \\ -e_{12} + e_{10} + e_{15} = 0 \\ e_{RT1} = e_{12} = \phi_{RT1} [(1-y_1)f_{12} + y_1 Df_1] \\ f_{RT1} = f_{12} = (1-y_1) \phi_{RT1}^{-1} (e_{12}) + y_1 Df_1 \end{cases} \quad (18)$$

The ARR are obtained from the behavioral model of the system through different procedures of the unknown variables elimination. The equations generated from the junctions are detailed in the appendix of this paper.

C. Generation of the ARRs

Each ARR is associated with a sensor, a component and a fault code. They are also described by a different equation linking all the above. The details of each ARR are provided in table IV.

TABLE IV. GENERATION OF ARRS

Faults code	Sensors used	Components monitored	Combinations of sensors placement	Analytical Redundancy Relations
ARR ₁	Df1, De3	RT1 and CV	00001010000000	$ARR_1 : -\varphi_{RT1} [Df_1] + \left[\frac{1}{s} \varphi_{CV}^{-1} (f_4) \right] + De_3 = 0$
ARR ₂	Df1, De3	CT1	00010000000000	$ARR_2 : -\varphi_{CT1} [sDe_3] + Df_1 + Df_1^* + Df_2^* = 0$
ARR ₃	Df3	CTS, RTS and CV	01100010000000	$ARR_3 : -\varphi_{RTS} [Df_3] + \left[\frac{1}{s} \varphi_{CV}^{-1} f_4 \right] + \frac{1}{s} \varphi_{CTS}^{-1} (f_{21}) = 0$
ARR ₄	De4	RT3 and CT3	00000001100000	$ARR_4 : -\varphi_{CT3} [sDe_4] - \varphi_{RT3}^{-1} (e_{34}) - Df_3^* - Df_4^* = 0$
ARR ₅	Df4	R and CTS	11000000000000	$ARR_5 : -\varphi_R [Df_4] + \left[\frac{1}{s} \varphi_{CTS}^{-1} f_{21} \right] - De_1^* = 0$
ARR ₆	De6, Df5	C1 and RT3	00000101000000	$ARR_6 : -\varphi_{C1} [sDe_6] + \varphi_{RT3}^{-1} (e_{34}) + Df_5 + Df_5^* + Sf_{36} + Sf_{37} = 0$
ARR ₇	Df10, De10	C1 and R1	00000000010001	$ARR_7 : -\varphi_{R1} [Df_{10}] + \left[\frac{1}{s} \varphi_{C1}^{-1} f_{55} \right] + De_{10} + Se_1 = 0$
ARR ₈	Df9	C1, C1, C2 and R2	00000100011010	$ARR_8 : -\varphi_{R2} [Df_9] - \left[\frac{1}{s} \varphi_{C2}^{-1} f_{53} \right] + \frac{1}{s} \varphi_{C1}^{-1} (f_{55}) + \frac{1}{s} \varphi_{C1}^{-1} (f_{39}) = 0$
ARR ₉	Df8, De10	C2 and R3	00000000001100	$ARR_9 : -\varphi_{R3} [Df_8] - \left[\frac{1}{s} \varphi_{C2}^{-1} f_{53} \right] + De_{10} + Se_{43} = 0$
ARR ₁₀	De10	CR	00000000100000	$ARR_{10} : -\varphi_{CR} [sDe_{10}] - Sf_0^v + Sf_1^i - Sf_{57} = 0$

Table IV shows that the chosen sensors are capable of monitoring all components of the system.

VI. SIMULATION SETUP

The simulations will focus on the sensitivity of two different sensors, Df1 and Df3. The tests with the Df1 will consist of simulating a leakage fault on it between the instant t= 2mn and t= 4mn on the component RT1. In the simulation setup of Df3, it will experience a fault between t= 2mn and t= 4mn.

A. Simulation Results for the Df1 Detector

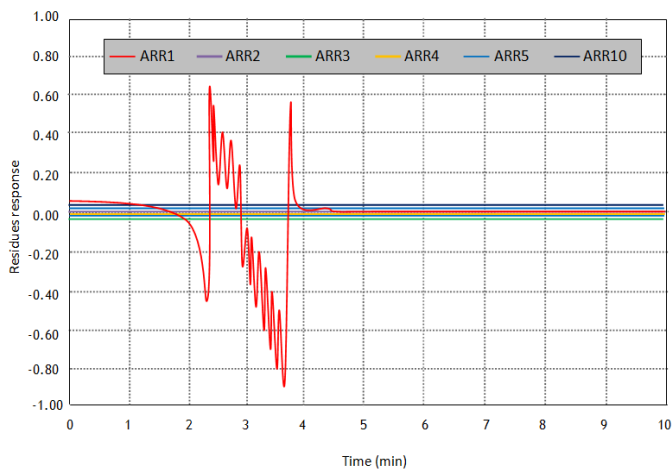


Figure 10. Sensitivity of detector Df1

Figure 9 shows six residues, ARR1 through ARR5 and ARR10. The failure in RT1 is characterized by the presence of the Df1 detector in the analytical redundancy relation ARR1. It

is possible to note that the residue ARR1 is sensitive to the failures which affect RT1, while the others remain unchanged.

B. Simulation Results for the Df3 Detector

Figure 10 shows the response of the residues ARR1 through ARR6 for this setup. The residue ARR3 presents a change between t1=2mn and t2=4mn and returns to its initial state. Other residues remain invariant.

These results confirm the capacity of ARR3 to detect faults in the RTS component.

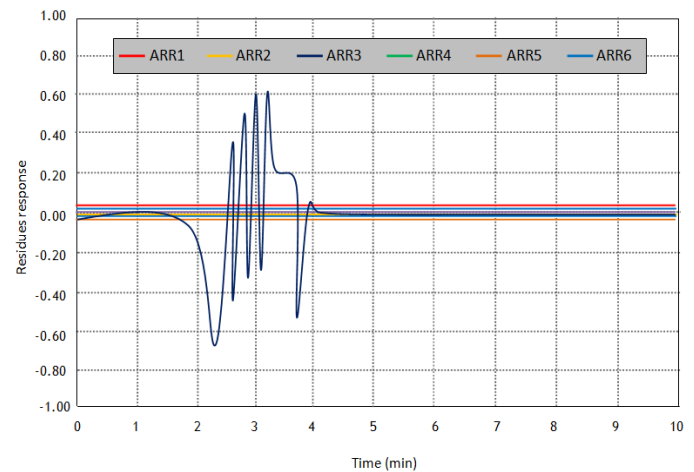


Figure 11. Sensitivity of Df3 detector

VII. CONCLUSION

The bond graph methodology is a convenient and useful tool for obtaining a monitoring model and a behavioral model for complex and non-linear systems.

This paper illustrates how bond graphs can be used for monitoring the dynamic transition of processes, in this case the operations in a distillation column.

Bond graphs were used to model the physical behavior of the system and then expanded to describe the monitoring system.

This expansion allows the optimal placement of sensors through the definition and use of Analytical Redundancy

$$ARR_1 : -\phi_{CV} [s\{(1-x_1)e_3 + x_1De_1\}] + Sf_1 + Sf_2 = 0$$

$$ARR_2 : -\phi_{RT1} [(1-y_1)f_{12} + y_1Df_1] + \left[\frac{1}{s}(1-x_2)\phi_{CV}^{-1}f_4 + x_2De_2 \right] + \frac{1}{s}(1-x_3)\phi_{CT1}^{-1}(f_{14}) + x_3De_3 = 0$$

$$ARR_3 : -\phi_{CV} [s\{(1-x_2)e_4 + x_2De_2\}] - (1-y_3)\phi_{RTS}^{-1}(e_8) - y_3Df_3 - (1-y_1)\phi_{RT1}^{-1}(e_{12}) + y_1Df_1 - Df_7 + Sf_5 + Sf_6 = 0$$

$$ARR_4 : -\phi_{RT3} [(1-y_2)f_{34} + y_2Df_2] + \left[\frac{1}{s}(1-x_4)\phi_{CT3}^{-1}f_{18} + x_4De_4 \right] - \frac{1}{s}(1-x_6)\phi_{Cl}^{-1}(f_{38}) - x_6De_6 = 0$$

$$ARR_5 : -\phi_{CT1} [s\{(1-x_3)e_{14} + x_3De_3\}] + (1-y_1)\phi_{RT1}^{-1}(e_{12}) + y_1Df_1 + Df_1^* + Df_2^* = 0$$

$$ARR_6 : -\phi_{RTS} [(1-y_3)f_8 + y_3Df_3] + \left[\frac{1}{s}(1-x_2)\phi_{CV}^{-1}f_4 + x_2De_2 \right] + \frac{1}{s}(1-x_5)\phi_{CTS}^{-1}(f_{21}) + x_5De_5 = 0$$

$$ARR_7 : -\phi_{CT3} [s\{(1-x_4)e_{18} + x_4De_4\}] - (1-y_2)\phi_{RT3}^{-1}(e_{34}) + y_2Df_2 - Df_3^* - Df_4^* = 0$$

$$ARR_8 : -\phi_R [(1-y_4)f_{23} + y_4Df_4] + \left[\frac{1}{s}(1-x_5)\phi_{CTS}^{-1}f_{21} + x_5De_5 \right] - De_1 = 0$$

$$ARR_9 : -\phi_{CTS} [s\{(1-x_5)e_{21} + x_5De_5\}] - (1-y_4)\phi_R^{-1}(e_{23}) - y_4Df_4 + (1-y_3)\phi_{RTS}^{-1}(e_8) + y_3Df_3 - Df_5^* = 0$$

$$ARR_{10} : -\phi_{Cl} [s\{(1-x_6)e_{38} + x_6De_6\}] + (1-y_2)\phi_{RT3}^{-1}(e_{34}) + y_2Df_2 + (1-y_5)\phi_{R2}^{-1}(e_{51}) + y_5Df_{10} + Df_5^* + Sf_{36} + Sf_{37} = 0$$

$$ARR_{11} : -\phi_{Cl} [s\{(1-x_7)e_{39} + x_7De_7\}] - \frac{1}{s}(1-x_7)\phi_{Cl}^{-1}(f_{39}) - y_7De_7 + Sf_{40} + Sf_{41} = 0 \quad (19)$$

$$ARR_{12} : -\phi_{R1} [(1-y_5)f_{51} + y_5Df_{10}] + \left[\frac{1}{s}(1-x_8)\phi_{Cl}^{-1}f_{55} + x_8De_8 \right] + \frac{1}{s}(1-x_{10})\phi_{CR}^{-1}(f_{58}) + x_{10}De_{10} - \frac{1}{s}(1-x_6)\phi_{Cl}^{-1}(f_{38}) - x_6De_6 + Se_1 = 0$$

$$ARR_{13} : -\phi_{R2} [(1-y_6)f_{48} + y_6Df_9] - \left[\frac{1}{s}(1-x_9)\phi_{C2}^{-1}f_{53} + x_9De_9 \right] + \frac{1}{s}(1-x_8)\phi_{Cl}^{-1}(f_{55}) + x_8De_8$$

$$+ \frac{1}{s}(1-x_7)\phi_{Cl}^{-1}(f_{39}) + x_7De_7 = 0$$

$$ARR_{14} : -\phi_{R3} [(1-y_7)f_{45} + y_7Df_8] - \left[\frac{1}{s}(1-x_9)\phi_{C2}^{-1}f_{53} + x_9De_9 \right] + \frac{1}{s}(1-x_{10})\phi_{CR}^{-1}(f_{58}) + x_{10}De_{10} + Se_{43} = 0$$

$$ARR_{15} : -\phi_{Cl} [s\{(1-x_8)e_{54} + x_8De_8\}] - (1-y_6)\phi_{R2}^{-1}(e_{48}) - y_6Df_9 - (1-y_5)\phi_{R1}^{-1}(e_{51}) - y_5Df_{10} + Sf_{54} = 0$$

Relations or ARRs. By following the method described in this paper, the ARRs were directly determined from the bond graph model.

The physical model was validated through the comparison of simulation and measurement results. The optimal sensors placement was validated through simulation of component failure and showed consistency with expected results.

VIII. APPENDIX - ARRs

From equations of junctions we generate the following ARRs:

$$ARR_{16} : -\phi_{C2} [s\{(1-x_9)e_{53} + x_9De_9\}] + (1-y_6)\phi_{R2}^{-1}(e_{48}) + y_6Df_9 - \phi_{R3} [(1-y_7)f_{45} + y_7Df_8] + Sf_{52} = 0$$

$$ARR_{17} : -\phi_{CR} [s\{(1-x_{10})e_{58} + x_{10}De_{10}\}] - (1-y_7)\phi_{R3}^{-1}(e_{45}) + y_7Df_8 - Sf_0^V + Sf_1^I - Sf_{57} = 0$$

REFERENCES

- [1] D. Muhammad, Z. Ahmad and N. Aziz, implementation of internal model control (imc) in continuous distillation column, Proc. of the 5th International Symposium on Design, Operation and Control of Chemical Processes, PSE ASIA 2010. Singapore July 25-28, 2010.
- [2] A. Vasičkaninová, M. Bakošová, Neural Network Predictive Control of a Chemical Reactor, Acta Chimica Slovaca, Vol.2, No.2, pp. 21-36, 2009.
- [3] J. C. MacMurray and D. Himmelblau, "Modeling and control of a packed distillation column using artificial neural networks," Computers & chemical engineering, vol. 19, pp. 1077-1088, 1995.
- [4] Z. Abdullah, et al., "Nonlinear modelling application in distillation column," Chemical Product and Process Modeling, vol. 2, 2007.
- [5] H. Bloemen, et al., "Wiener model identification and predictive control for dual composition control of a distillation column," Journal of Process Control, vol. 11, pp. 601-620, 2001.
- [6] P. Kadlec, et al., "Data-driven soft sensors in the process industry," Computers & chemical engineering, vol. 33, pp. 795-814, 2009.
- [7] X. Wang, et al., "Designing a soft sensor for a distillation column with the fuzzy distributed radial basis function neural network," in Decision and Control, 1996, Proceedings of the 35th IEEE, 1996, pp. 1714-1719.
- [8] F. D. C. Corazza, et al., "Application of a subdivision algorithm for solving nonlinear algebraic systems-DOI: 10.4025/actascitechnol. v30i1. 3198," Acta Scientiarum. Technology, vol. 30, pp. 27-38, 2008.
- [9] A. D. Kroumov, et al., "Desenvolvimento de um modelo da cinética enzimática da transesterificação de óleos vegetais para produção de biodiesel-DOI: 10.4025/actascitechnol. v29i1. 79," Acta Scientiarum. Technology, vol. 29, pp. 9-16, 2007.
- [10] J. Fernandez de Canete, P. Del Saz Orozco and S. Gonzalez-Perez, Distillation Monitoring and Control using LabVIEW and SIMULINK Tools, World Academy of Science, Engineering and Technology, International Journal of Computer, Information, Systems and Control Engineering Vol:1 No:10, 2007.
- [11] M. Khemliche, et al., "Sensor placement for component diagnosability using bond-graph," Sensors and Actuators A: Physical, vol. 132, pp. 547-556, 2006.
- [12] W. Borutzky, "Bond graph modelling and simulation of multidisciplinary systems—an introduction," Simulation Modelling Practice and Theory, vol. 17, pp. 3-21, 2009.
- [13] B. A. Brooks, "Modeling of a distillation column using bond graphs," the university of Arizona, 1993.
- [14] P. M. Frank, "Fault diagnosis in dynamic systems using analytical and knowledge-based redundancy: A survey and some new results," Automatica, vol. 26, pp. 459-474, 1990.
- [15] V. Venkatasubramanian, et al., "A review of process fault detection and diagnosis: Part III: Process history based methods," Computers & chemical engineering, vol. 27, pp. 327-346, 2003.
- [16] P. J. Feenstra, et al., "Bond graph modeling procedures for fault detection and isolation of complex flow processes," SIMULATION SERIES, vol. 33, pp. 77-84, 2001.
- [17] M. Tagina, et al., "Monitoring of systems modelled by bond-graphs," SIMULATION SERIES, vol. 27, pp. 275-275, 1994.
- [18] A. Fijany and F. Vatan, "A new efficient method for system structural analysis and generating analytical redundancy relations," in Aerospace conference, 2009 IEEE, pp. 1-12, 2009.